Supplementary Information: Marine Organic Aerosol Reflect Ecosystem Variability from Phytoplankton Functional Types to Micronekton

Emmanuel Chevassus[1], Vaios Moschos[1], Kirsten N. Fossum[1], Lu Lei[1], Liz Coleman[1], Dagmar B. Stengel[1], Vignesh Prabhu[1], Wei Xu[1+], Darius Ceburnis[1], Colin O' Dowd[1], Jurgita Ovadnevaite[1]

[1] School of Natural Sciences, Ryan Institute's Centre for Climate and Air Pollution Studies, University of Galway, H91 TK33, Co. Galway, Ireland

[+] Now at Institute of Urban Environment, Chinese Academy of Sciences, Xiamen 361021

Correspondence to: Jurgita Ovadnevaite (jurgita.ovadnevaite@universityofgalway.ie)

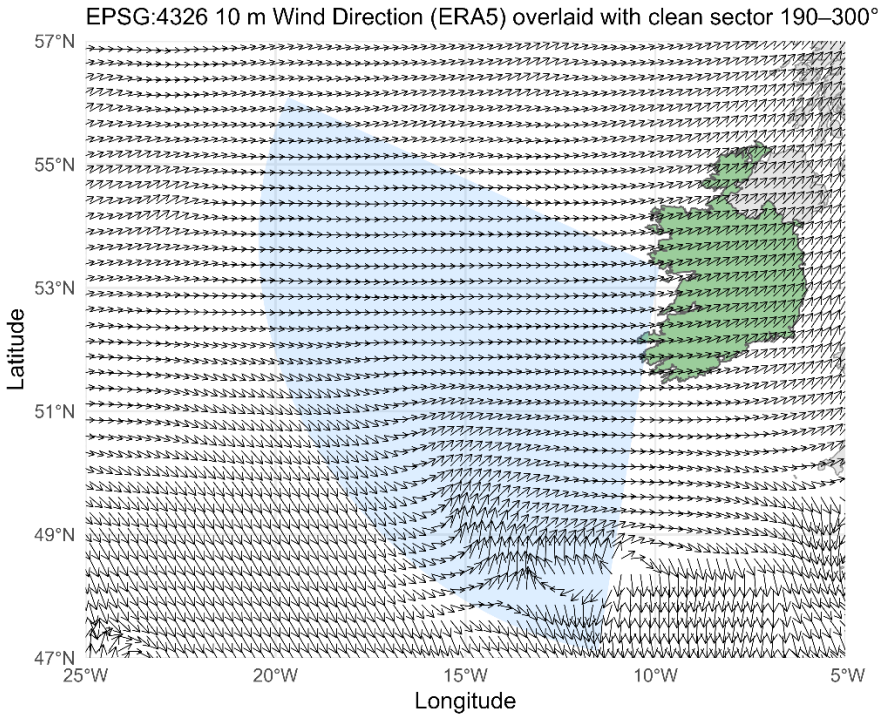

Figure S1. Mace Head clean sector (190-300°) overlaid with ERA5 10m wind direction quivers for a typical summertime clean period.

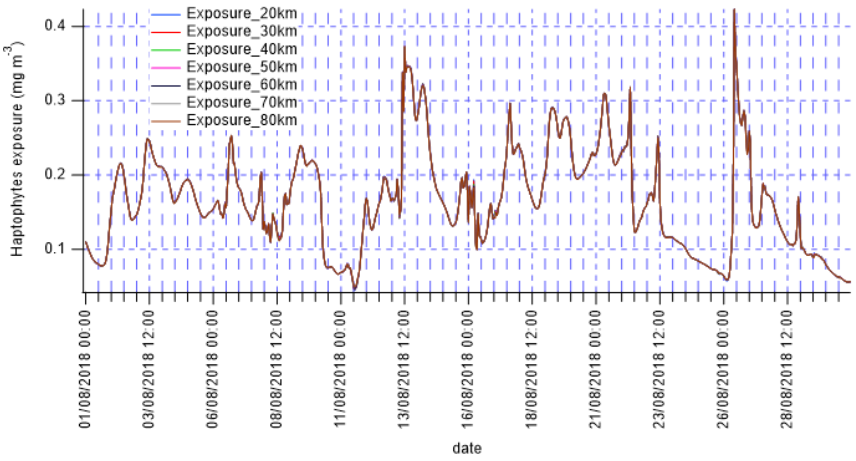

Figure S2. PFTs air-mass exposure was calculated by integrating surface concentrations along back trajectories using circular sampling radii of 20, 40, 60, and 80 km around each HYSPLIT trajectory point to check for spatial sampling scale sensitivity.

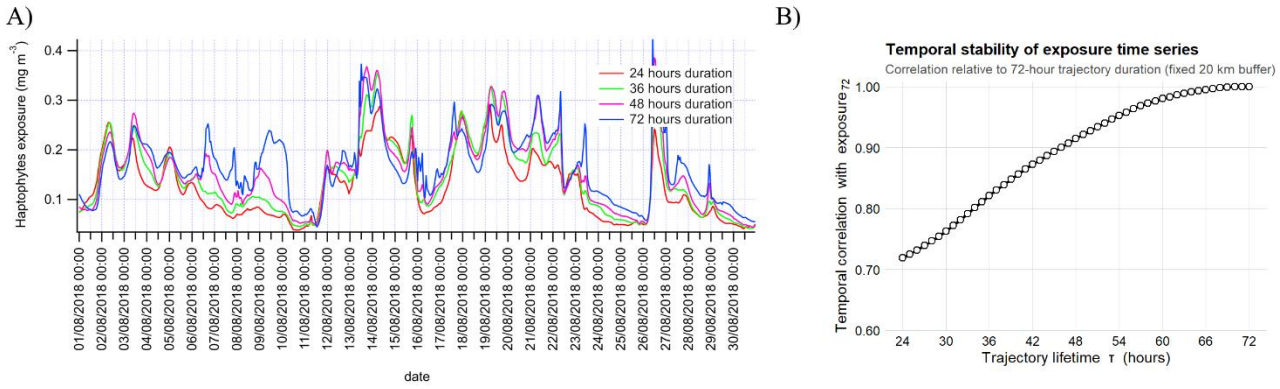

Figure S3. Sensitivity of haptophytes exposure to trajectory lifetime. A) Time series using back-trajectories durations of 24 h (red), 36 h (magenta), 48 h (green) and 72 h (blue). B) Temporal correlation (Pearson´s R) between exposure time series computed with each duration τ and the 72-h reference case.

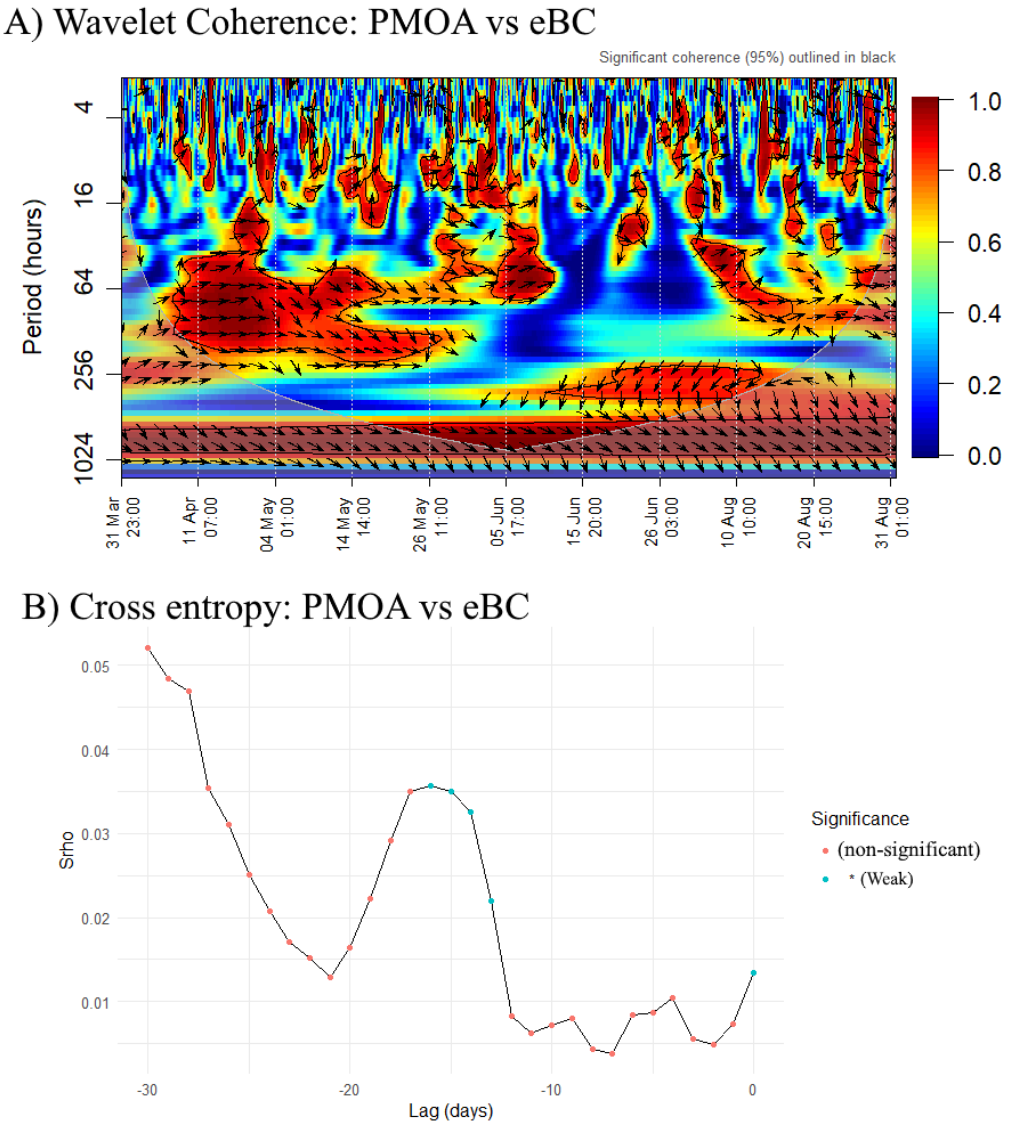

Figure S4. (A) Cross-wavelet coherence between primary marine organic aerosol (PMOA) and elemental black carbon (eBC) during 2018. Colours indicate the magnitude of wavelet coherence (0-1), with black contours denoting regions significant at the 95% confidence level against red-noise. Arrows represent phase relationships (right: in-phase; left: anti-phase; up/down: lead-lag). The cone of influence (grey shading) marks regions affected by edge effects. (B) Lagged cross-entropy between PMOA and eBC. The Significance markers distinguish non-significant and weakly significant lags; the absence of a sharp highly significant, isolated minimum indicates no robust or stable lead-lag relationship.

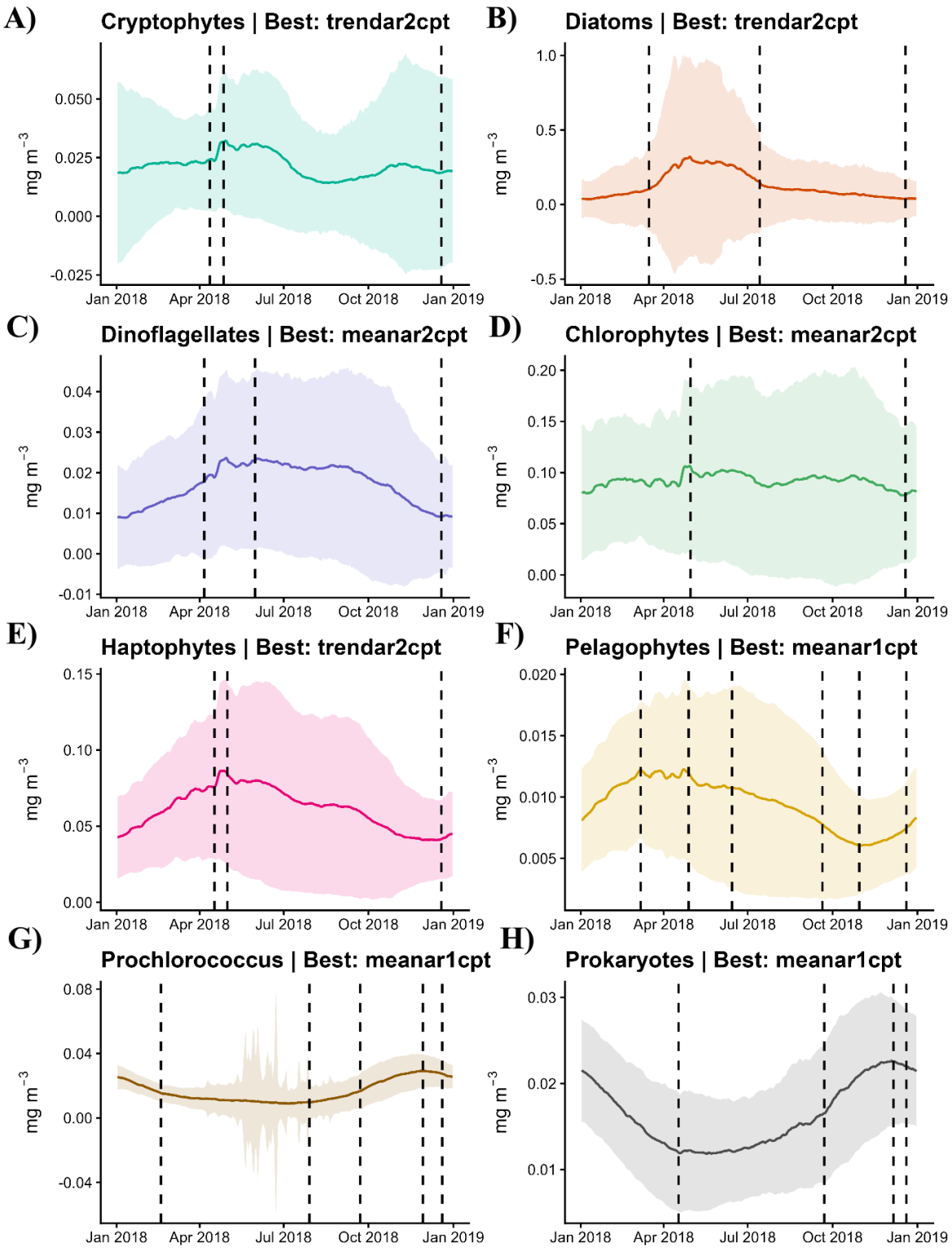

Figure S5. Daily Temporal dynamics of phytoplankton functional types in the North Atlantic extracted from the AIGD-PFT model (Zhang *et al*. 2024). Yearly time series of chl-*a* biomass (mg m⁻³) for major phytoplankton functional types averaged over the region bounded by 20°-66°N and 72°W-0° longitude, similarly to Mansour *et al*. (2024). Panels show: (A) Cryptophytes, (B) Diatoms, (C) Dinoflagellates, (D) Chlorophytes, (E) Haptophytes, (F) Pelagophytes, (G) *Prochlorococcus*, (H) Other Prokaryotes. Shaded areas represent variability (standard deviation) around the mean (negative values are not meaningful), vertical dashed lines denote detected changepoints.

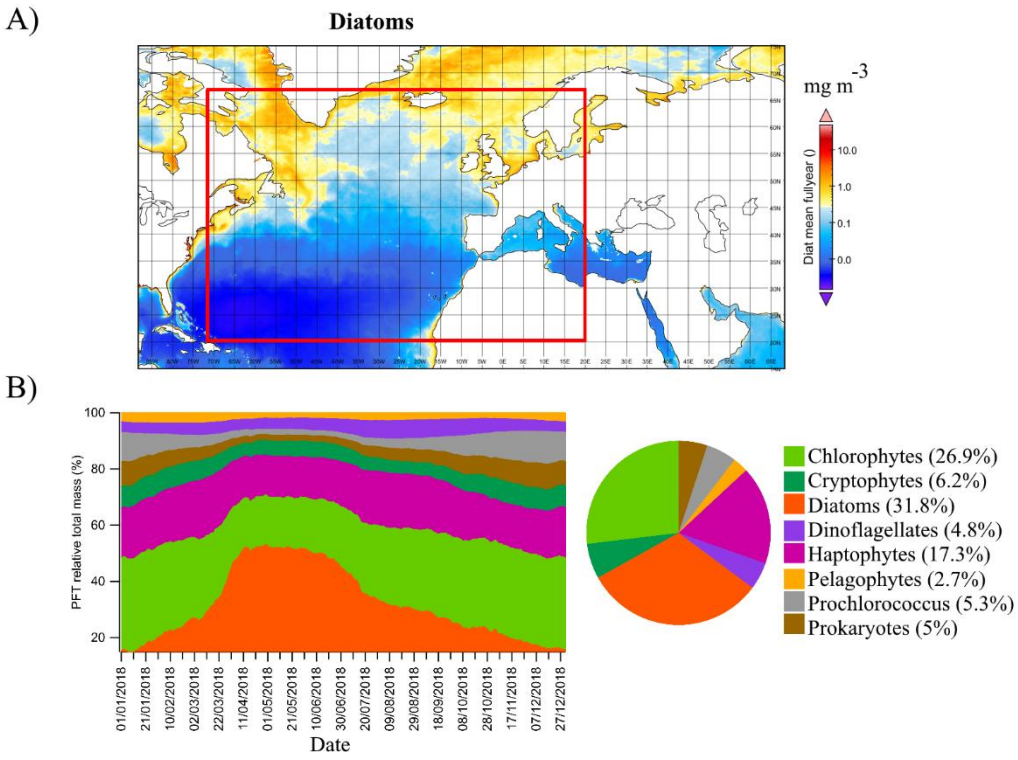

Figure S6. (A) AIGD-PFT Annual mean diatom mass concentrations averaged over the region 20°-66° N, 72° W-0° E. (B) Relative contributions of individual phytoplankton functional types to total chlorophyll-a biomass (sum of the 8 PFTs) within the same region.

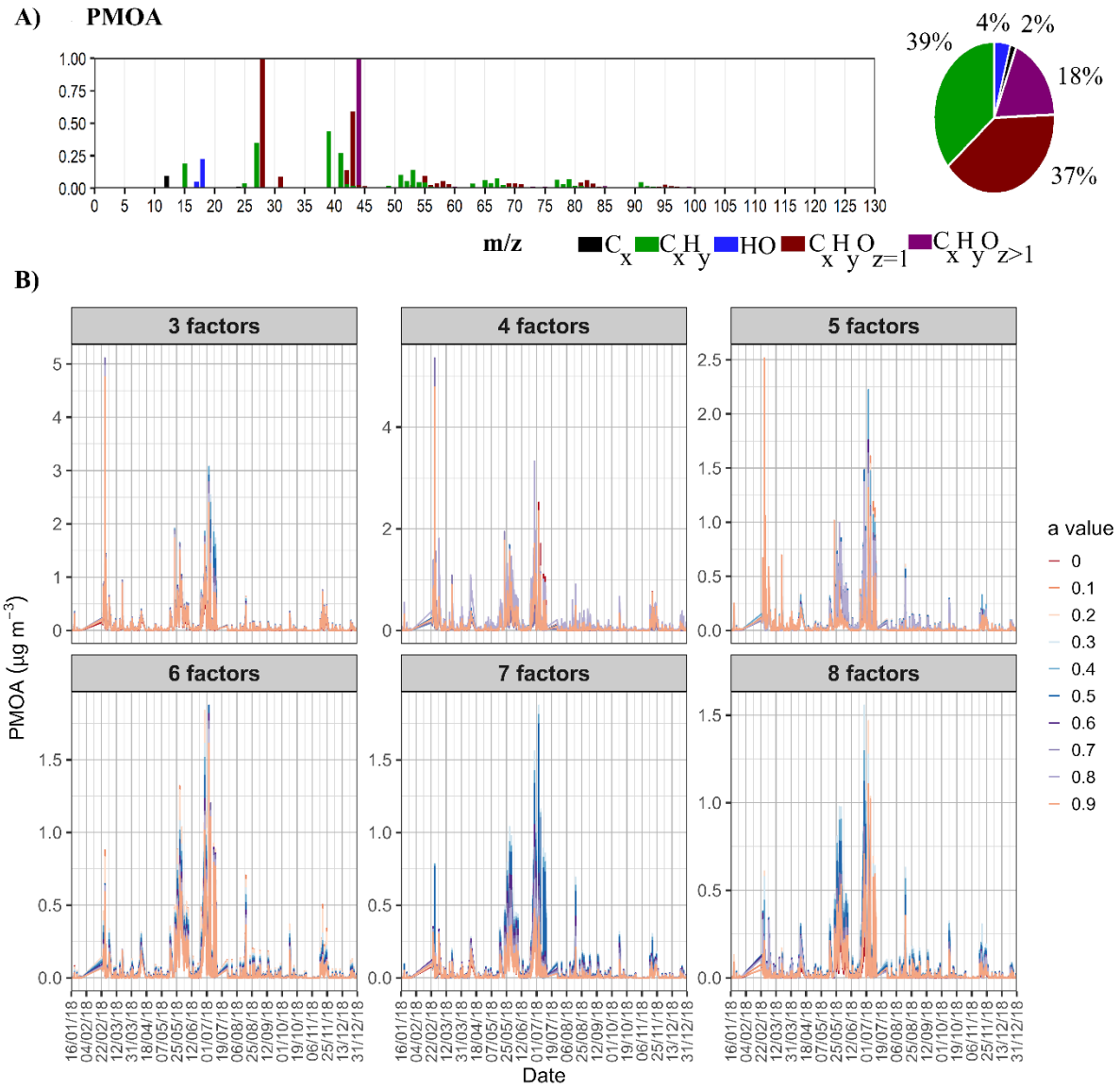

Figure S7. (A) Mass spectra constrained using the Ovadnevaite *et al.* (2011) reference profile. (B) Corresponding PMOA (µg m⁻³) time series reconstructed from PMF solutions ranging from 3 to 8 factors, with a-value variation (0–0.9)

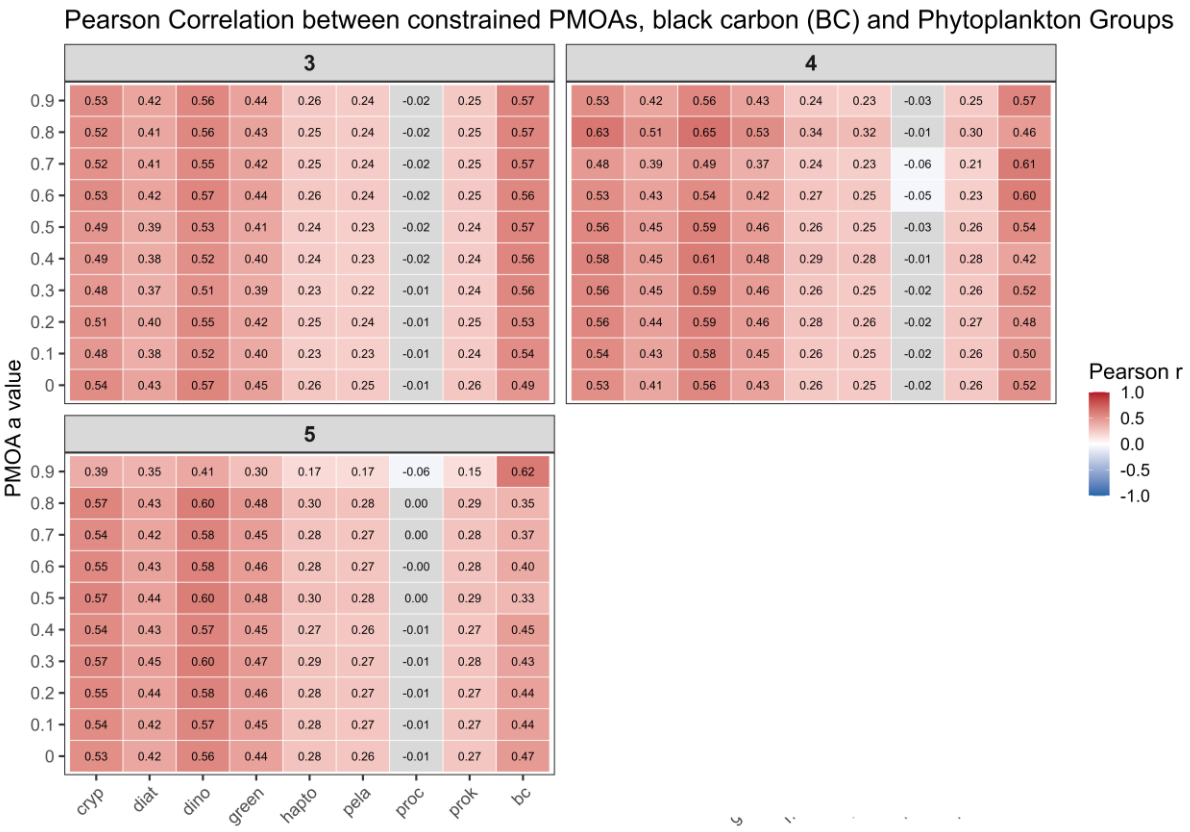

Figure S8. Pearson correlations between constrained PMOA time series and phytoplankton functional types (PFTs) and black carbon (BC) for PMF solutions within 3 to 5 factors. Rows show the a-value used to constrain the PMOA reference spectrum and columns the external variables. Values indicate Pearson correlation coefficients (R). Colours denote significant correlations ($p < 0.05$), while non-significant correlations are shown in grey.

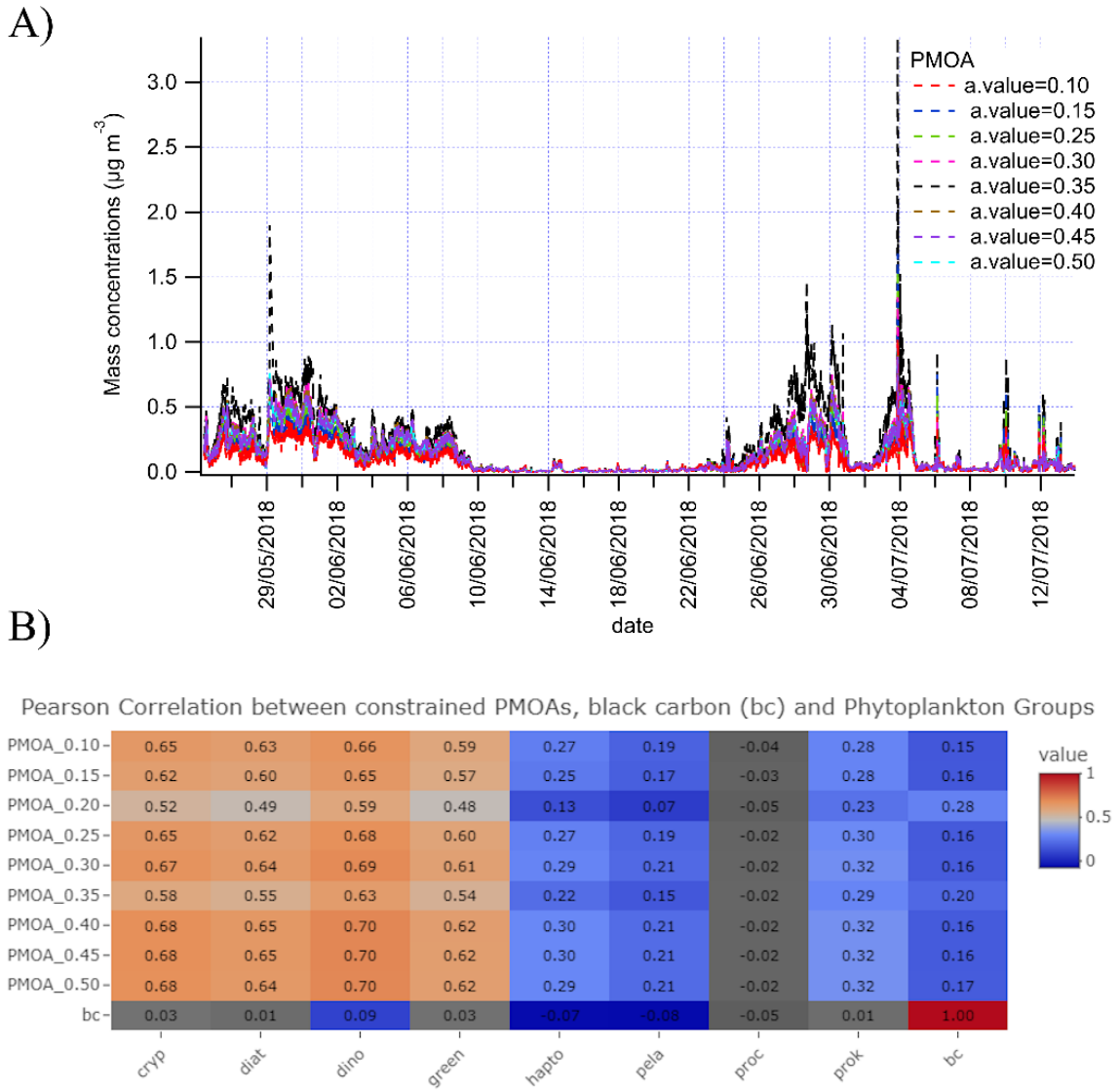

Figure S9. A) Primary marine organic aerosol (PMOA) sensitivity to a-values constraining B) Retained PMOA time series (a-value of 0.40) along with Phytoplankton functional types exposure with retained phytoplankton functional types (cryptophytes, dinoflagellates, diatoms and chlorophytes). B) Pearson´s correlations between primary marine organic aerosol (PMOA) constraining sensitivity analysis time series (a-values), black carbon (bc) and phytoplankton functional types exposure time series, non-significant correlations (p-values>0.05) are represented as grey shaded cells.

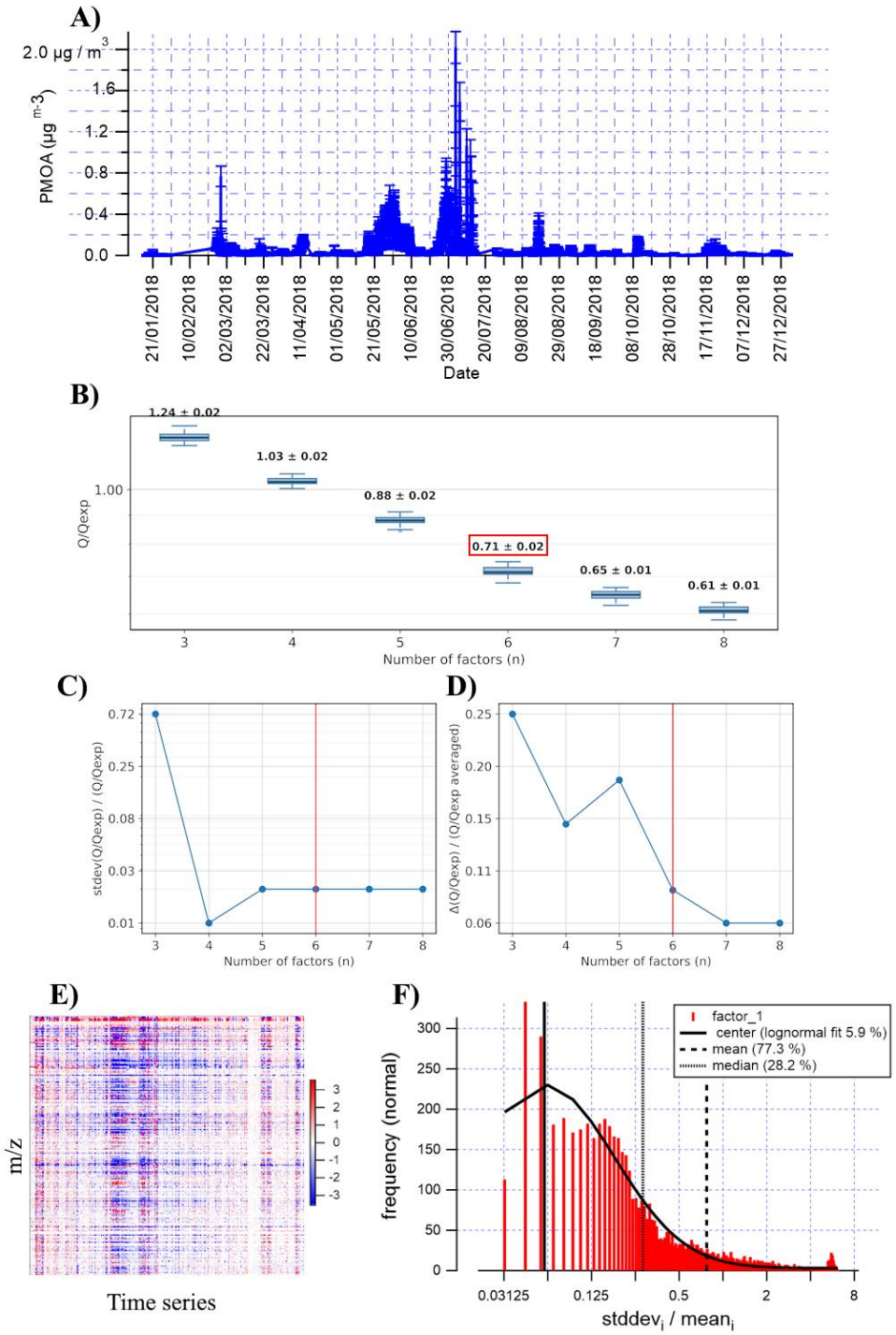

Figure S10. (A) PMOA time series (μg m⁻³) from the six-factor solution, expressed as the mean ± standard deviation across all bootstrap runs. (B) Distribution of Q/Qexp across bootstrap runs for factor solutions ranging from three to eight factors, with mean ± standard deviation indicated above each box. (C) Relative variability of Q/Qexp, expressed as the standard deviation divided by the mean across bootstrap runs, as a function of factor number. (D) Relative change in Q/Qexp between successive factor solutions, defined as Δ(Q/Qexp)/⟨Q/Qexp⟩ from n to n+1 factors. (E) Scaled residuals matrix (observed minus modelled) for the six-factor solution, (F) Distribution of relative uncertainty across bootstrap runs, with lognormal fit (solid line), mean (dashed line) and median (dotted line) indicated.

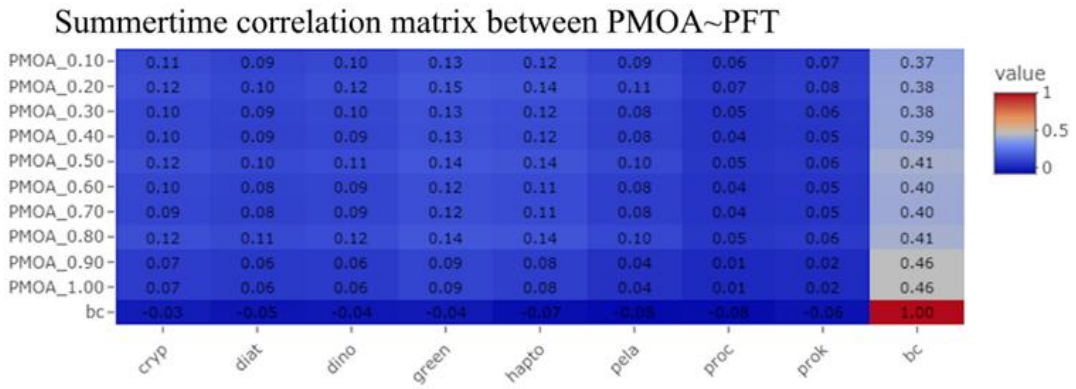

Figure S11. August 2018 - Pearson's correlations between primary marine organic aerosol (PMOA) constraining sensitivity analysis time series (a-values), black carbon (bc) and phytoplankton functional types HYSPLIT air masses exposure time series, non-significant correlations (p-values>0.05) are represented as grey shaded cells. Black carbon measurements are used as a counterfactual against truly pristine conditions.

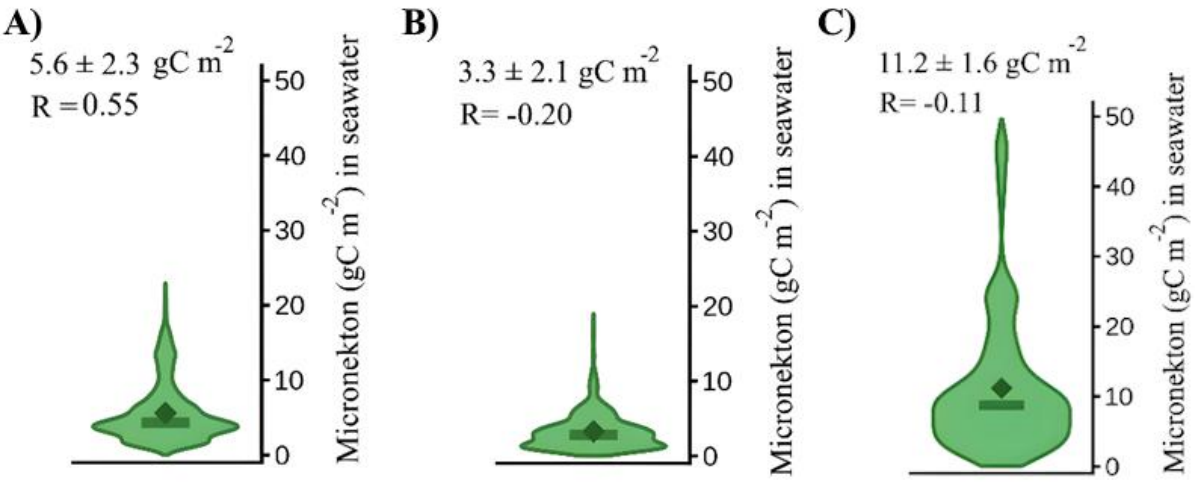

Figure S12. Violin plots show the distribution of micronekton biomass (gC m^{-2} in seawater) air masses exposure, with the horizontal bar indicating the median and the diamond the geometric mean. Values above each violin report the geometric mean ± geometric standard deviation.

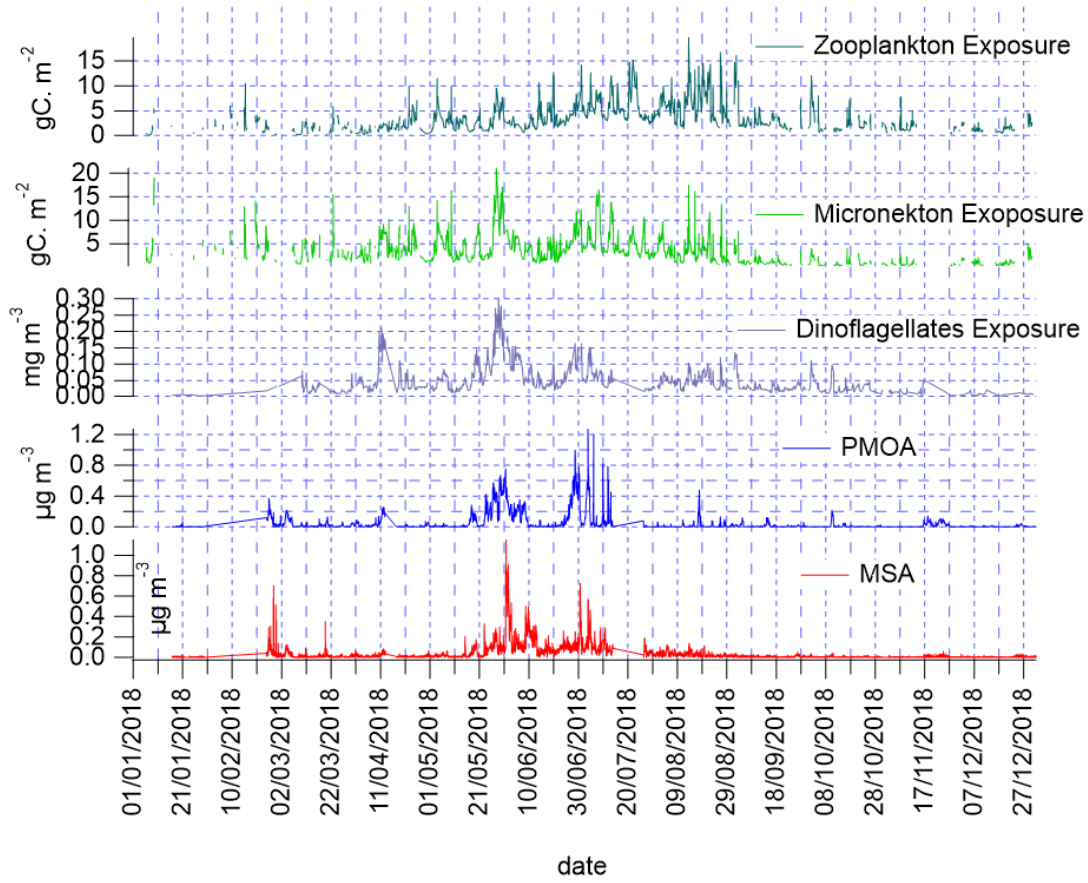

Figure S13. Time series of air-mass-integrated zooplankton and epipelagic micronekton exposure (gC m^{-2}), dinoflagellate exposure (mg m^{-3}), primary marine organic aerosol (PMOA, µg m^{-3}), and methane-sulphonic acid organic aerosol (MSA, µg m^{-3}) at Mace Head during 2018.

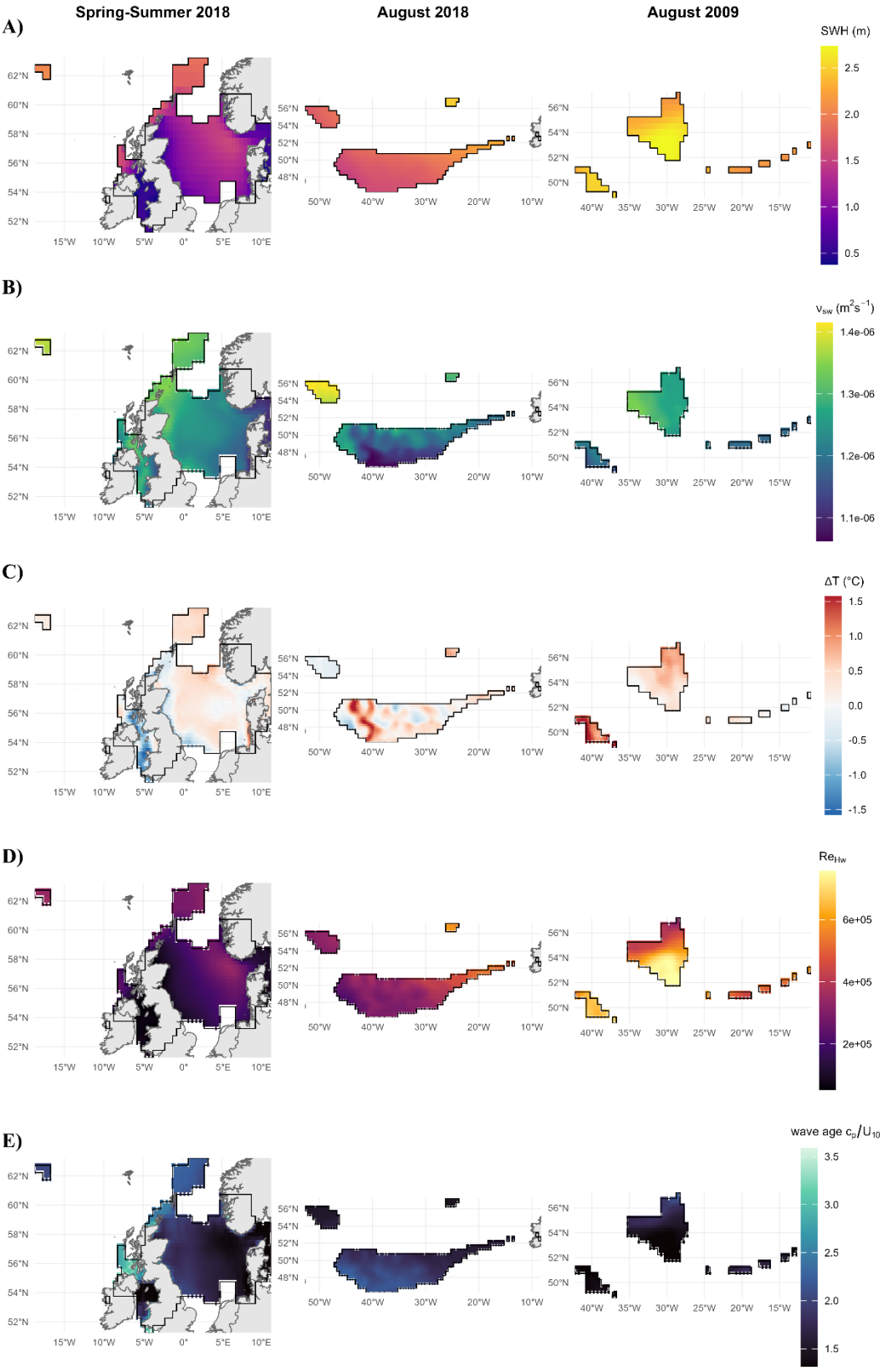

Figure S14. Wave-physical and atmospheric parameters along HYSPLIT sources for the three case study periods (Spring–Summer 2018, August 2018, August 2009). (A) Total significant wave height H_s (m); (B) seawater kinematic viscosity ν_sw (m² s⁻¹); (C) air-sea temperature difference ΔT (°C), (D) wave Reynolds number Re_Hw; (E) wave age c_p/U_10.

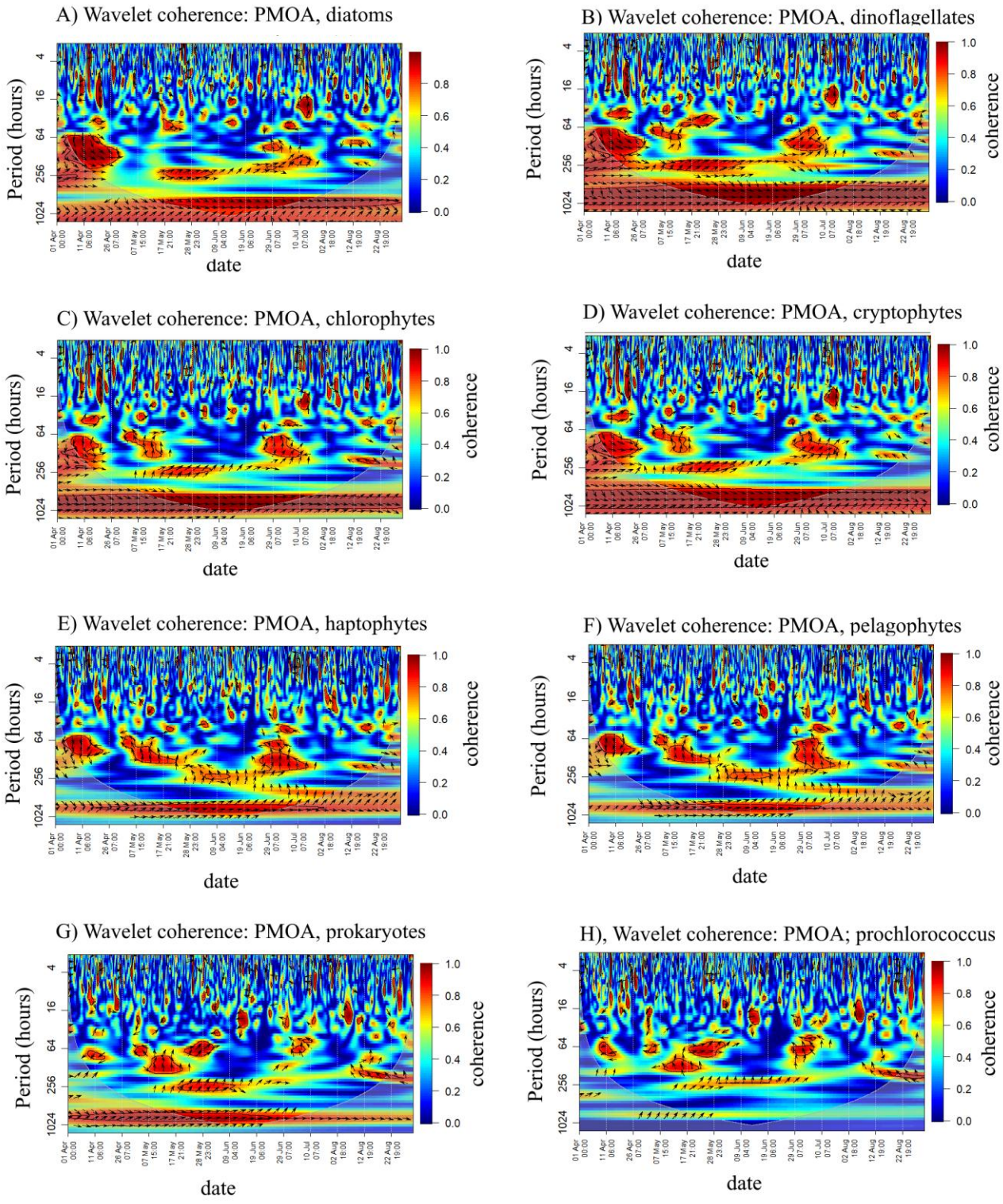

Figure S15. Continuous wavelet coherence spectra between particulate marine organic aerosol (PMOA) mass concentrations and major phytoplankton functional types over the spring-summer 2018 climax period. Panels show (A) Diatoms, (B) Dinoflagellates, (C) Chlorophytes, (D) Cryptophytes, (E) Haptophytes, (F) Pelagophytes, (G) Prokaryotes, and (H) P*rochlorococcus*.

Warm colours indicate regions of high coherence (0–1), black contours enclose statistically significant areas at the 95 % confidence level based on Monte Carlo permutations.

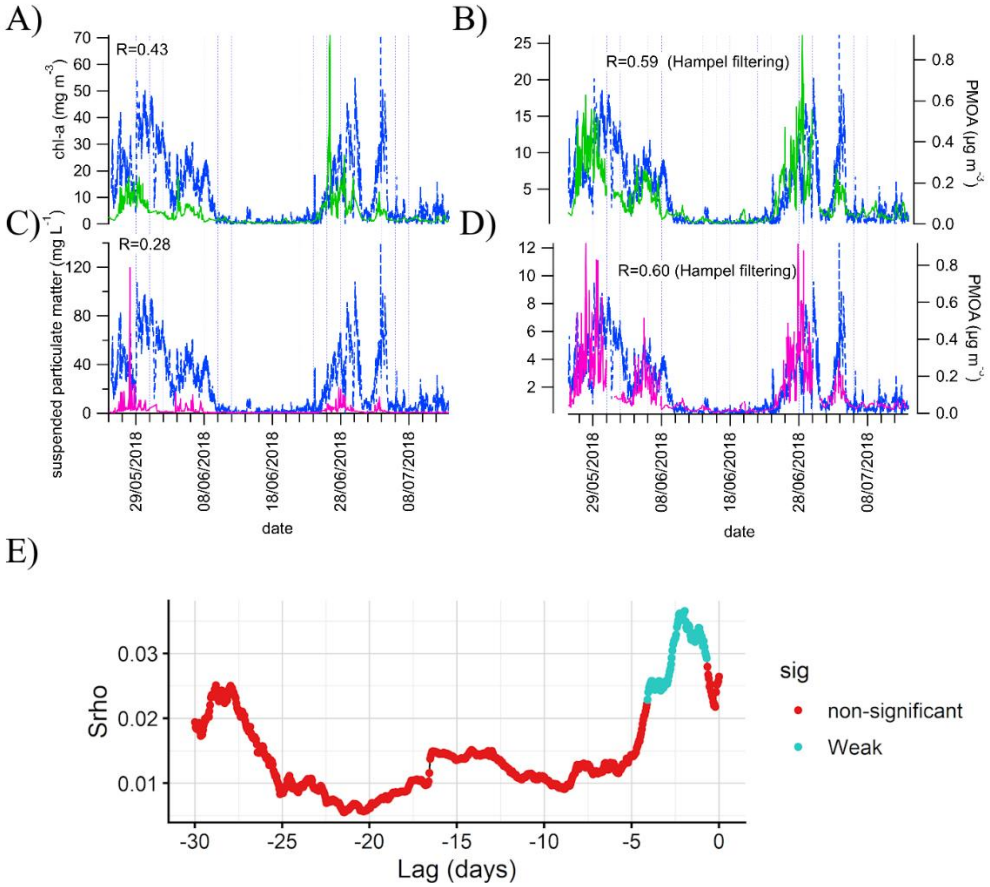

Figure S16. Time series of satellite-derived ocean colour variables compared with PMOA during the spring-summer climax period. Panels show (A) chlorophyll-*a* (chl-*a*), (B) Hampel-filtered chl-*a*, (C) suspended particulate matter (SPM), and (D) Hampel-filtered SPM, F) Cross entropy between PMOA and Hampel filtered chl-*a*.

Table S1. Longhurst Regional variability in PFT composition

Region	Cryptophytes (%)	Diatoms (%)	Dinoflagellates (%)	Chlorophytes (%)	Haptophytes (%)	Pelagophytes (%)	*Prochloroccus* (%)	Prokaryotes (%)	Total (mg m^{-3})
NADR	6.9	24.4	5.0	31.1	23.7	3.1	3.3	2.5	0.48
ARCT	5.2	49.4	4.6	18.0	18.7	2.4	0.9	0.8	0.97
NECS	5.2	49.4	4.6	18.0	18.7	2.4	0.9	0.8	0.90
NWCS	8.7	53.9	5.2	20.7	6.7	1.0	2.0	1.8	0.83

Region	Cryptophytes (%)	Diatoms (%)	Dinoflagellates (%)	Chlorophytes (%)	Haptophytes (%)	Pelagophytes (%)	*Prochlorococcus* (%)	Prokaryotes (%)	Total (mg m^{-3})
SARC	5.6	45.0	5.4	22.8	17.4	2.0	0.8	1.0	0.77
BPLR	7.2	65.5	4.2	15.7	4.7	0.9	1.3	0.6	0.97
NASE	7.0	19.4	4.3	32.3	22.2	3.2	6.2	5.4	0.36
GFST	6.3	22.9	4.6	30.8	18.4	2.8	7.6	6.7	0.31

Table S2. Pearson´s correlations between different phytoplankton groups and sea spray related measurements (PMOA in this study) across marine regions; data compiled from Moallemi *et al.* (2021a)[1], Jung *et al.* (2020)[2], Freney *et al.* (2020)[3], Trueblood *et al.* (2021)[4], Schwier *et al.* (2017)[5], Schwier *et al.* (2015)[6] and (Sellegri *et al.*, 2021)[7]. NS: non-significant

PFT measurements	This Study HR-ToF-AMS	Southern Ocean[1] SSF	Amundsen Sea[2] SSF	Med Sea[3] ToF-ACSM	Med Sea[4] INP	Med Sea[5] CCN	Med Sea[6] CCN	Med Sea[7] CCN
Cryptophytes	0.68			-0.22	0.48	0.58		
Diatoms	0.65		0.89			0.64		
Dinoflagellates	0.70	-0.4 0.4				0.64		
Chlorophytes	0.62	0.55 0.69						
Haptophytes	0.30	-0.4 0.4		-0.27–0.38	0.10–0.48			0.32
Pelagophytes	0.21	0.44						
Prochlorococcus	-0.02	-0.4 0.4					0.70	
Prokaryotes	0.32	-0.4 0.4		-0.41–0.28	NS			
Micronekton	0.55							

HR-ToF-AMS: High-Resolution Time-of-Flight Aerosol Mass Spectrometer; SSF: Sea Spray Fluorescence; ToF-ACSM: Time-of-Flight Aerosol Chemical Speciation Monitor; INP: Ice Nucleating Particles; CCN: Cloud Condensation Nuclei; NS: Not significant.

References

Freney, E., Sellegri, K., Nicosia, A., Trueblood, J.T., Rinaldi, M., Williams, L.R., Prévôt, A.S.H., Thyssen, M., Grégori, G., Haëntjens, N., Dinasquet, J., Obernosterer, I., Van-Wambeke, F., Engel, A., Zäncker, B., Desboeufs, K., Asmi, E., Timmonen, H., Guieu, C., 2020. Mediterranean nascent sea spray organic aerosol and relationships with seawater biogeochemistry (preprint). Aerosols/Field Measurements/Troposphere/Chemistry (chemical composition and reactions). https://doi.org/10.5194/acp-2020-406

Jung, J., Hong, S.-B., Chen, M., Hur, J., Jiao, L., Lee, Y., Park, K., Hahm, D., Choi, J.-O., Yang, E.J., Park, J., Kim, T.-W., Lee, S., 2020. Characteristics of methanesulfonic acid, non-sea-salt sulfate and organic carbon aerosols over the Amundsen Sea, Antarctica. Atmos. Chem. Phys. 20, 5405–5424. https://doi.org/10.5194/acp-20-5405-2020

Mansour, K., Decesari, S., Ceburnis, D., Ovadnevaite, J., Russell, L.M., Paglione, M., Poulain, L., Huang, S., O'Dowd, C., Rinaldi, M., 2024. IPB-MSA&SO_4 : a daily 0.25° resolution dataset of in situ-produced biogenic methanesulfonic acid and sulfate over the North Atlantic during 1998–2022 based on machine learning. Earth Syst. Sci. Data 16, 2717–2740. https://doi.org/10.5194/essd-16-2717-2024

Moallemi, A., Landwehr, S., Robinson, C., Simó, R., Zamanillo, M., Chen, G., Baccarini, A., Schnaiter, M., Henning, S., Modini, R.L., Gysel-Beer, M., Schmale, J., 2021. Sources, Occurrence and Characteristics of Fluorescent Biological Aerosol Particles Measured Over the Pristine Southern Ocean. JGR Atmospheres 126, e2021JD034811. https://doi.org/10.1029/2021JD034811

Ovadnevaite, J., O'Dowd, C., Dall'Osto, M., Ceburnis, D., Worsnop, D.R., Berresheim, H., 2011. Detecting high contributions of primary organic matter to marine aerosol: A case study. Geophysical Research Letters 38. https://doi.org/10.1029/2010GL046083

Schwier, A.N., Rose, C., Asmi, E., Ebling, A.M., Landing, W.M., Marro, S., Pedrotti, M.-L., Sallon, A., Iuculano, F., Agusti, S., Tsiola, A., Pitta, P., Louis, J., Guieu, C., Gazeau, F., Sellegri, K., 2015. Primary marine aerosol emissions from the Mediterranean Sea during pre-bloom and oligotrophic conditions: correlations to seawater chlorophyll *a* from a mesocosm study. Atmos. Chem. Phys. 15, 7961–7976. https://doi.org/10.5194/acp-15-7961-2015

Schwier, A.N., Sellegri, K., Mas, S., Charrière, B., Pey, J., Rose, C., Temime-Roussel, B., Jaffrezo, J.-L., Parin, D., Picard, D., Ribeiro, M., Roberts, G., Sempéré, R., Marchand, N., D'Anna, B., 2017. Primary marine aerosol physical flux and chemical composition during a nutrient enrichment experiment in mesocosms in the Mediterranean Sea. Atmos. Chem. Phys. 17, 14645–14660. https://doi.org/10.5194/acp-17-14645-2017

Sellegri, K., Nicosia, A., Freney, E., Uitz, J., Thyssen, M., Grégori, G., Engel, A., Zäncker, B., Haëntjens, N., Mas, S., Picard, D., Saint-Macary, A., Peltola, M., Rose, C., Trueblood, J., Lefevre, D., D'Anna, B., Desboeufs, K., Meskhidze, N., Guieu, C., Law, C.S., 2021. Surface ocean microbiota determine cloud precursors. Sci Rep 11, 281. https://doi.org/10.1038/s41598-020-78097-5

Trueblood, J.V., Nicosia, A., Engel, A., Zäncker, B., Rinaldi, M., Freney, E., Thyssen, M., Obernosterer, I., Dinasquet, J., Belosi, F., Tovar-Sánchez, A., Rodriguez-Romero, A., Santachiara, G., Guieu, C., Sellegri, K., 2021. A two-component parameterization of marine ice-nucleating particles based on seawater biology and sea spray aerosol measurements in the Mediterranean Sea. Atmos. Chem. Phys. 21, 4659–4676. https://doi.org/10.5194/acp-21-4659-2021

Zhang, Y., Shen, F., Li, R., Li, M., Li, Z., Chen, S., Sun, X., 2024. AIGD-PFT: the first AI-driven global daily gap-free 4 km phytoplankton functional type data product from 1998 to 2023. Earth Syst. Sci. Data 16, 4793–4816. https://doi.org/10.5194/essd-16-4793-2024